Lab on a Chip

RSC Publishing

PAPER

View Article Online
View Journal | View Issue

Cite this: *Lab Chip*, 2013, **13**, 3225

Surface acoustic waves for on-demand production of picoliter droplets and particle encapsulation†

David J. Collins,[a] Tuncay Alan,[a] Kristian Helmerson[b] and Adrian Neild*[a]

Received 21st March 2013,
Accepted 30th May 2013

DOI: 10.1039/c3lc50372k

www.rsc.org/loc

Microscopic water-in-oil droplets are a versatile chemical and biological platform whose dimensions result in short reaction times and require minuscule amounts of reagent. Methods exist for the production of droplets, though the vast majority are only able to do so in continuous flows, restricting the ability to independently control reactions of individual droplets, a prerequisite for programmable digital microfluidics. Here we present a novel method to produce individual picoliter-scale droplets on-demand using surface acoustic waves (SAW). Acoustic forces arising from SAW act on the oil–water interface, creating a droplet whose volume is defined by the applied power, duration of the force and system geometry. Additionally, this method is able to pre-concentrate particles simultaneously with droplet production, meaning that particles and cells, even if in a dilute mixture, can be easily encapsulated. Our method is expected to be applicable to high-throughput screening, bioreactor creation and other microfluidic processes.

Introduction

Over the past decade there has been a growing interest to develop miniaturized high throughput screening (HTS) platforms[1,2] that can replace the full functionality of microtitre plate technology on a single chip for improved efficiency and reduced costs.[3,4] This expectation, along with the recent advances in microfluidics, has attracted significant attention to droplet based systems to encapsulate reagents and targets[5,6] such as proteins or cells[7,8] into nano-to-pico-liter volumes, for subsequent reaction, transport and analysis in an enclosed microscale system.[9]

Working with samples at such small length scales enables different reagents in different concentrations to be assayed, promising orders of magnitude reduction in both the amount of reagents and the time scales compared with conventional processes.[10,11] Similarly, (1) concentration gradients that may be undesirable in a single-fluid microfluidic system can be avoided, with different phases of fluid – usually oil and water – acting as a barrier to diffusion and, (2) using a droplet as a chamber for a reaction in a two-fluid-phase microfluidic device with droplet production and analysis components integrated on-chip also allows these processes to be performed without the need for fluid handling, with the fleetingly small reaction volumes reducing the need to perform separate mixing steps. Further, nanoliter droplets encapsulating cells and particles in nanoliter volumes[7] produced in a digital microfluidic device can be used as bioreactors,[8,12,13] though until now the ability to concentrate and produce encapsulated particles on demand for a digital microfluidic device has remained elusive.

Different methods have been developed for the purpose of producing droplets in microfluidic systems, where significant effort has been made to develop and characterize T-junctions[10,14–16] and flow-focusing systems.[17,18] To produce droplets a continuous fluid flow of two immiscible fluids (typically oil and water) are required, with a constant stream of monodisperse droplets resulting from the combination of these two fluid streams. Technologies used to drive these flows, most often peristaltic pumps or syringe pumps, dispense constant flow rates but are poorly suited to accurate manipulation of discrete volumes in the sub-nanoliter range, making on-demand production of individual droplets difficult to control. Further, in most microfluidic devices the pressure gradient source is located distances away from the device that are orders of magnitude larger than the length scales of that device, introducing time delays and additional reagent volumes and causing pressure gradients to depend on the length of connecting tubing.

For digital microfluidic systems to be able to produce droplets on-demand pressure gradients should be discretely controlled on-chip. Methods that have the demonstrated ability to create localized pressure gradients sufficient to deform a fluid interface include electrowetting arrays,[19,20] electrohydrodynamic,[21] pyroelectrohydrodynamic jetting[22] and piezoelectric acoustic devices.[23–27] These mechanisms have been applied for open air droplet movement, though are

[a]*Department of Mechanical and Aerospace Engineering, Monash University, Clayton, VIC 3800, Australia. E-mail: adrian.neild@monash.edu; Tel: +61 3 990 54655*
[b]*School of Physics, Monash University, Clayton, VIC 3800, Australia*

† Electronic supplementary information (ESI) available: Interface deformation modeling (Discussion 1) and videos of droplet production (Video 1) and particle encapsulation (Videos 2 and 3). See DOI: 10.1039/c3lc50372k

limited in relevance to high-throughput systems by factors including large minimum reaction volume, slow translocation speed, requirement for a fluid-air interface and difficulty integrating the actuation components into a planar microfluidic system. However, acoustic forces are unusual in that they can create a time-averaged force on both fluid-fluid interfaces [27–29] and particles,[30–33] creating the possibility for these two activities to be integrated in the same device. The ability for the acoustic force to affect fluids differently based on their physical properties also allows for their use in two-phase fluid systems, in contrast to open-air systems subject to evaporation and undesired droplet coalescence. Surface acoustic waves (SAWs) are uniquely placed among acoustic actuation technologies. A SAW device is created through the patterning of interdigital transducers (IDTs) on a piezoelectric substrate such as lithium niobate (LN). Compared to most bulk acoustic wave devices, devices using SAW have the advantages of (1) having acoustic energy localized at the surface, permitting efficient energy transfer to a fluid placed on top,[34] (2) being planar and therefore easily integrated with typically 2D microfluidic devices[35,36] and (3) operating at significantly higher frequencies (~10–1000 MHz) with a corresponding wavelength (4–400 μm) encompassing the length scales on most microfluidic devices. To date, these devices have been used for diverse applications including mixing,[37] concentration,[30,32,38] continuous flow pumping,[23,39] jetting[40] and atomization.[25]

Here we present a novel and flexible method for on-demand droplet generation in digital microfluidic systems using SAW. This technique incorporates the SAW device directly into the microfluidic platform and simultaneously integrates steps for concentration, encapsulation and droplet production.

System design and operating principle

The SAW droplet generation system is composed of a microfluidic chamber placed atop a SAW device, shown in (Fig. 1a). The SAW device is composed of a series of gold focused interdigital transducers (FIDTs) arrayed on a lithium niobate (LN) substrate, with the distance between each successive transducer determining the resonant frequency, *f*,

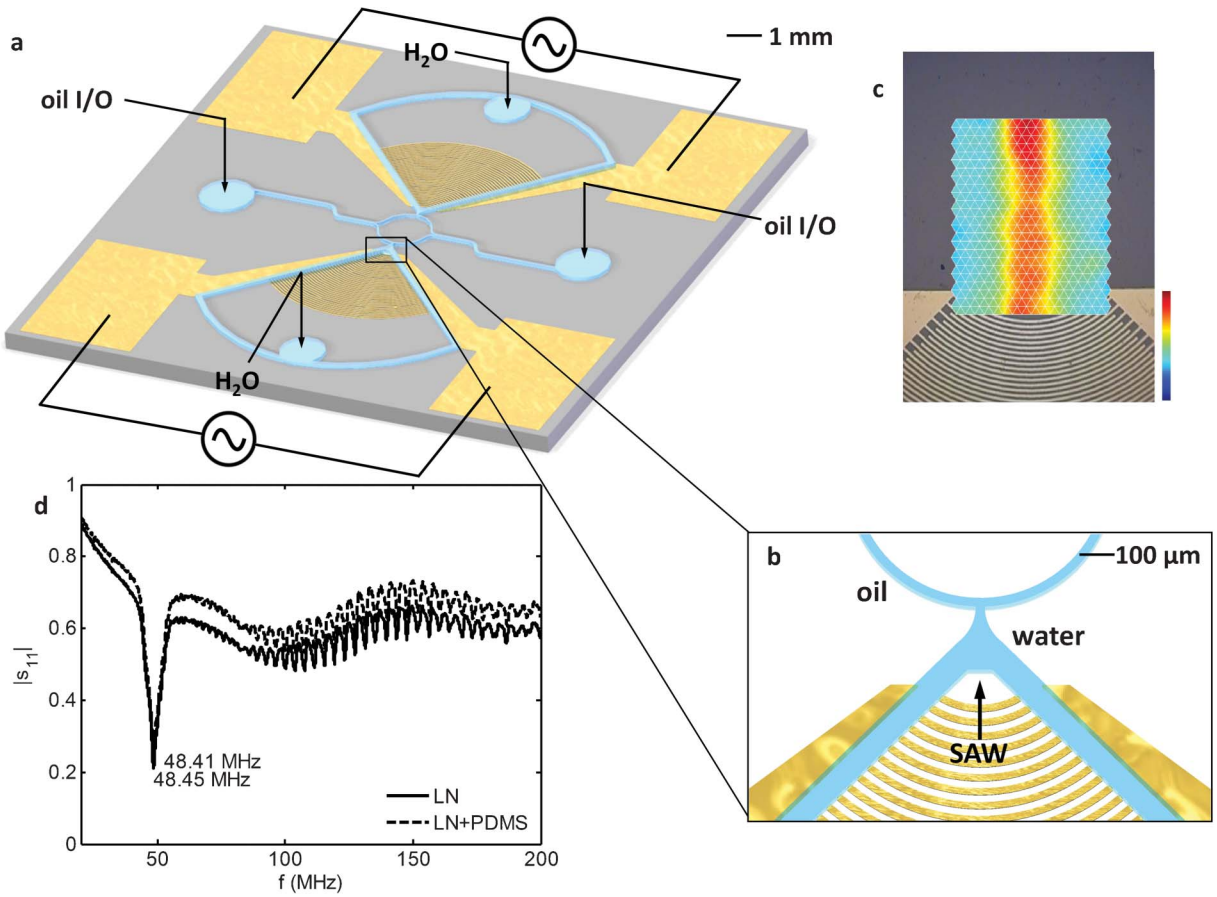

Fig. 1 Sketch of the SAW-controlled picoliter-scale droplet generation system. (a) A continuous oil phase is pumped in either symmetric oil inlet/outlet. Water is pumped in the inlets to the rear of the FIDTs until a steady water/oil interface at the microfluidic T-junction (see (b) inset) is maintained. Application of an AC signal across the electrode pads will produce a SAW, whose RMS amplitude distribution is visualized in (c), and which will act on the water–oil interface, pushing the water phase into the continuous oil phase to produce a water-in-oil droplet. (d) The resonant frequency of a SAW device is determined by its minimum reflection coefficient, or $|s_{11}|$. Loading PDMS atop a 80 μm device makes little difference to the resonant frequency.

of the device (Fig. 1d) according to $f = c_s/\lambda$, where c_s is the sound speed on the substrate surface and λ is the distance between FIDT finger-pairs. When an AC signal is applied across the transducers at this frequency the electromechanical displacement induced in the piezoelectric substrate creates a SAW, the displacement of which decays exponentially with depth into the substrate, attenuating almost completely in the first few wavelengths from the surface.[41]

The mechanics of SAW fluidics are well known: a SAW traveling at a substrate fluid interface will radiate acoustic energy into the fluid at the Rayleigh angle $\theta_R = \sin^{-1}(c_f/c_s)$, where c_f is the sound speed in the fluid. The acoustic wave, now traveling in the fluid, will continue traveling until encountering an interface with a medium of different acoustic properties. The acoustic pressure on an interface has been the focus of several publications by many prominent authors in the field of nonlinear acoustics.[42–45] Generally the acoustic radiation force on a surface in the path of an acoustic beam can here be broken up into what is called the Langevin and Rayleigh radiation pressures; the first of these refers to the time-averaged force tensor in the direction of acoustic propagation on a surface placed in the path of a beam, while the Rayleigh pressure on a surface is the combination of this and the isotropic static pressure induced. Both formulations of acoustic pressure are equally valid, though apply to different systems, depending on whether the interface the acoustic beam acts upon is suspended within a given fluid or is a physical barrier to a region with different acoustic properties. In the case of an acoustic beam acting on an oil–water interface in a closed system, there is no method to transfer the isotropic pressure induced by the beam to the oil side of the interface besides interface deformation, with the static pressure component contributing to that deformation. The Rayleigh pressure, p_r, acting on an interface is given by[43,44]

$$p_r = \langle p - p_0 \rangle + \langle \rho v^2 \rangle \quad (1)$$

where the brackets $\langle\rangle$ denote a time averaged quantity, p is the pressure in the fluid, p_0 is the initial (without acoustic actuation) pressure, ρ is the fluid density, v is the instantaneous fluid particle velocity and $\langle \rho v^2 \rangle$ is the energy density in the fluid $\langle E \rangle$. To a first approximation the fluid particle velocity $v \approx v_0$, where $v_0 = (\xi\omega)$ is the substrate velocity, ξ is the surface displacement and $\omega = 2\pi f$. If the substrate velocity is sinusoidally oscillating as in a SAW, the time average $\langle \rho v^2 \rangle$ is nonzero, resulting in a nonzero pressure term on an interface in the path of the acoustic beam. The static pressure component $\langle p - p_0 \rangle$ arises from the nonlinear propagation of the acoustic wave through the fluid, with the attenuation of acoustic energy in the wave equal to the increase in static pressure. Supplementary Discussion 1 describes and models the roles static and surface pressure arising from SAW have in deforming an oil–water interface.†

Methods

We employed 40 μm and 80 μm wavelength focused SAW devices, comprising 90 and 45 finger-pairs of 90° circular focussed interdigital transducers (FIDTs), respectively, on a 0.5 mm thick, single side polished 128° *Y-cut*, *X*-propagating lithium niobate (LN) substrate. The 10 nm chrome/200 nm aluminium FIDTs were aligned on the substrate with the SAW propagation oriented in the preferred propagation direction on the LN, as shown in Fig. 1. With the exception of the electrode pads, across which an AC signal is applied, the devices were further coated with 70 nm of evaporation-deposited SiO_2 to cover the IDTs and promote adhesion with polydimethylsiloxane (PDMS), which was bonded to the device after exposure to an activated air plasma (Harrick Plasma PDC-002, Ithaca, NY: 450 mTorr, 29.6W, 3 min for the SiO_2-coated LN substrate and 1.5 min for the PDMS). Bonding of the activated surfaces was enhanced by heating the joined surfaces (70 °C, 10 min) immediately following coupling. Several chamber geometries were explored, including devices where the IDTs were covered entirely by PDMS (results in Fig. 2a–e) or fluid (Fig. 2f–g, 3, 4). Both setups are capable of producing water-in-oil droplets, though higher powers are required to produce equivalent results when PDMS is bonded directly to the IDTs due to lossy SAW transmission at the LN-PDMS interface.[46]

Experiments were performed with the device stabilized on a 3D-printed platform and placed on the stage of a microscope (Olympus BX43, Tokyo, Japan) and imaged using a 5MP eyepiece camera (Dino-Lite AM7023B, New Taipei City, Taiwan). Olive oil (viscosity =85 cP, surface tension at oil–water interface is $\approx$0.024 N m^{-1}[47]), comprising the continuous flow stream, was injected into the device using a syringe pump (KD Scientific Legato 210, Holliston, MA, USA), whereas water was manually manipulated using a 1 mL syringe until a steady-state (flat) oil–water interface was achieved. The SAW was generated by applying a sinusoidal voltage across the electrode pads using a signal generator (BelektroniG F10, Freital, Germany) and amplifier. Surface velocity was measured and the traveling wave SAW was visualized in the vicinity of the FIDT focal point using a laser Doppler vibrometer (Polytech GmBH UHF-120, Waldbronn, Germany). Temperature measurements were made using a thermal imaging camera (FLIR i7, Meer, Belgium).

Results

Droplet generation

The simplest geometry for droplet production in microfluidic systems is the T-junction, where a continuous (oil) phase is intersected by a disperse (water) phase. In Fig. 2 a modified T-junction is integrated with a SAW device with the orifice located at the FIDT focal point. Application of SAW to the oil–water interface leads to interface deformation, extending the water into the oil phase leading to droplet production (see Supplementary Video 1). In the context of continuous droplet

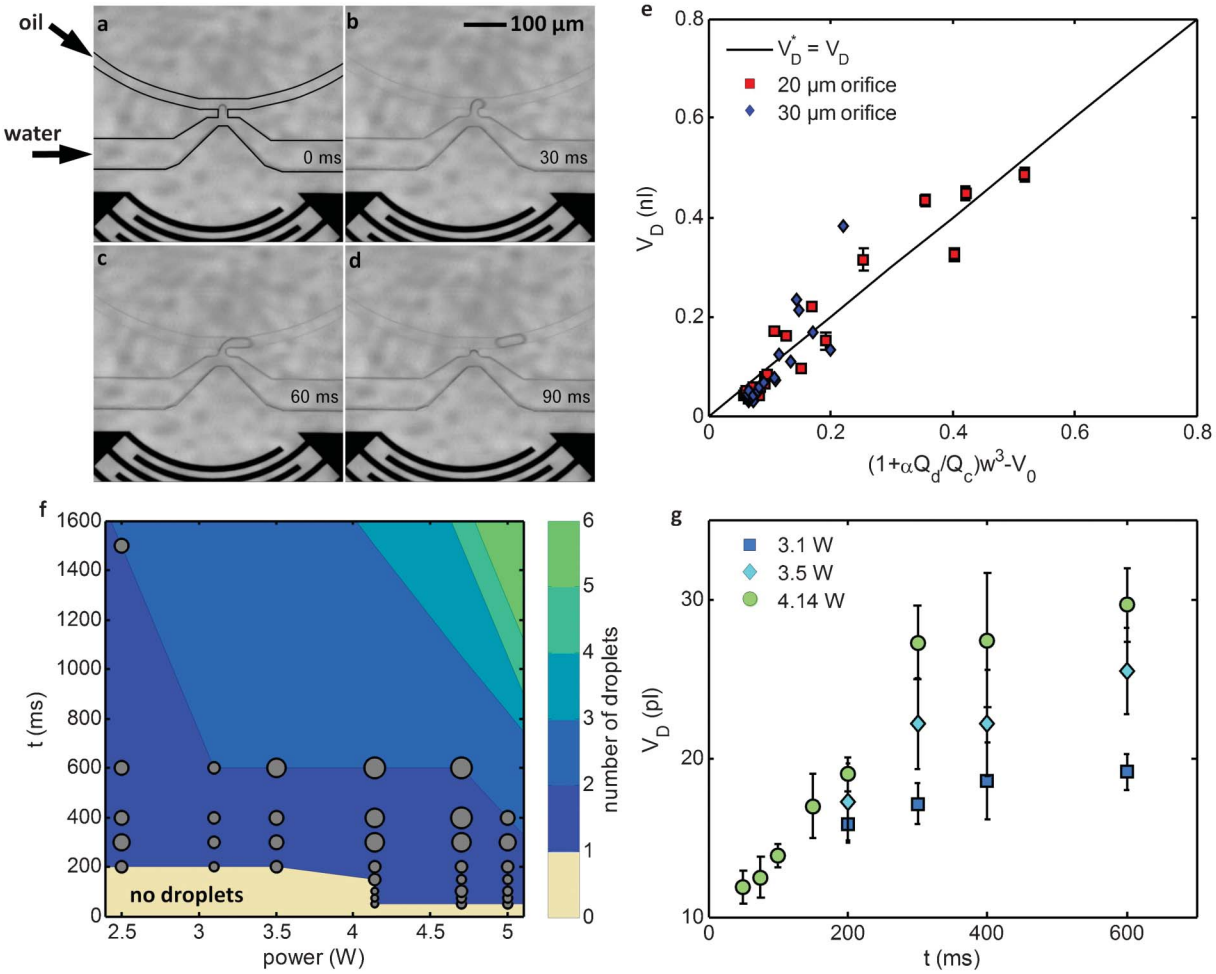

Fig. 2 (a–d) Images (~30 ms apart) of droplet production in a confined system comprised of a 20/30 μm width/height orifice and a 30/30 μm width/height circular channel of radius 745 μm, with (a) showing the water–oil interface immediately after application of SAW, (b–c) showing interface deformation due to acoustic pressure and channel cross flow, and (d) a fully formed droplet in channel. Droplet is produced when SAW of FIDT wavelength 80 μm is applied for 100 ms at 48.4 MHz, starting at (a) and ending at (c). (e) The droplet volume V_D produced with application of SAW is determined by flow rate in the channel. A constant pulse results in an outlet velocity of 2.1 ± 0.5 mm s^{-1}, resulting in a flow ratio Q_d/Q_c essentially solely determined by the oil flow rate. Incorporating Q_d/Q_c, where Q_d is inferred by the ejection rate of water into the oil stream, into eqn (3) yields a satisfactory comparison with measured droplet sizes. (f) The number of droplets produced using a 20/30 μm width/height orifice and channel is determined by the power level (2.5–5 W) and pulse duration (50–1500 ms). (g) The droplet volume (grey circles in (f)) is similarly determined by these factors, with increasing volume for increased power and duration, here shown for 3.1–4.14 W for the case where <2 droplets are produced.

production, the intrusion of the disperse phase into the continuous phase results in droplet break-off, a mechanism that has been well-covered in the existing literature.[14,48–50] The droplet breakup regime is determined by the capillary number Ca = $\mu u/\gamma$, where u is the velocity of the continuous phase in the channel, μ is the fluid viscosity and γ is the interfacial tension, with the critical capillary number Ca* ≈ 0.015 determining the transition from the so-called squeezing to dripping regimes.[14] The velocities characteristic to most microfluidic systems result in Ca < Ca*, where droplet size is unaffected by viscous shear and where droplet formation in a T-junction occurs in a roughly four-stage process: (1) a disperse phase fluid enters a continuous phase channel (Fig. 2a), (2) the disperse phase fills the width of the channel (Fig. 2b), (3) the pressure drop, arising from the thinning boundary layer in the continuous phase, lengthens the disperse phase drop and (4) the thinning neck at the boundary of the orifice (Fig. 2c) breaks to form a drop in the continuous phase channel (Fig. 2d). It is known from Garstecki *et al.* that in this regime the length of droplets in a channel is only determined by the channel geometry and flow rates of the continuous, Q_c, and disperse, Q_d, phases according to the expression[48]

$$\ell/w = 1 + \alpha Q_d/Q_c \quad (2)$$

where ℓ is the length of the drop in the channel, w is the channel width and α is a constant specific to the chamber geometry and of order unity. In a square channel, the predicted droplet volume $V_D^* \sim Lw^2$; subtracting the empty

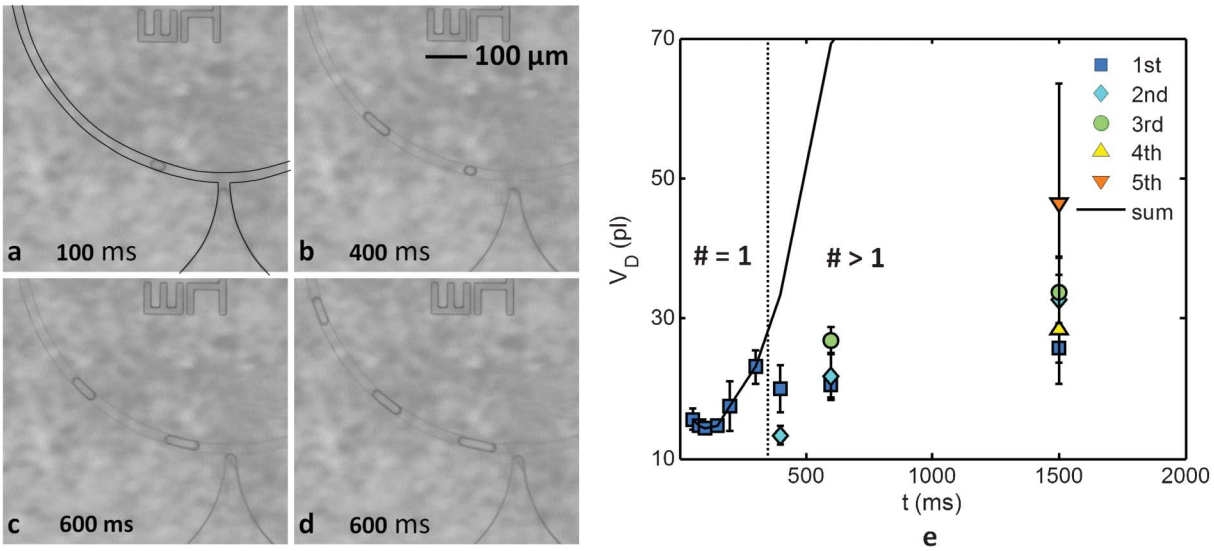

Fig. 3 (a–d) Images showing droplets that are produced for different pulse durations (100–600 ms), with (c) and (d) from the same droplet sequence shown 200 ms apart. (e) The droplet size produced during multi-droplet production is dependent on the duration of the pulse. For pulses less than ~350 ms in duration (here at 5 W), only one (# = 1) droplet is produced (see Fig. 2f). A pulse longer than that required to produce a single droplet can produce additional droplets (# > 1), though the volume of the last droplet in a series may be smaller than the initial droplet if the SAW pulse ceases during formation (b). If this does not occur, subsequent droplets will be larger, suggesting accelerating rates of interface deformation.

volumes at leading and trailing edges of the drop and assuming circular curvature at both ends yields $V_D^* \approx Lw^2 - V_0$, where the subtracted empty volume $V_0 = w^3(1 - \pi/6)$. Incorporating eqn (2), the volume of a drop in a channel is given by

$$V_D^* = w^3(\alpha Q_d/Q_c + \pi/6) \quad (3)$$

where Q_d here is determined by the rate of interface movement on application of SAW. Increasing power and duration results in larger droplets (Fig. 2g), here increasing the effective Q_d.

For a constant Q_c the ejected droplet volume is a function of both the applied power and SAW pulse duration. Finding that the water ejection velocity is constant for a given applied power, the droplet size for increasing flow velocities with $u = Q_c/w^2$ is found to agree with model in eqn (3), observed in

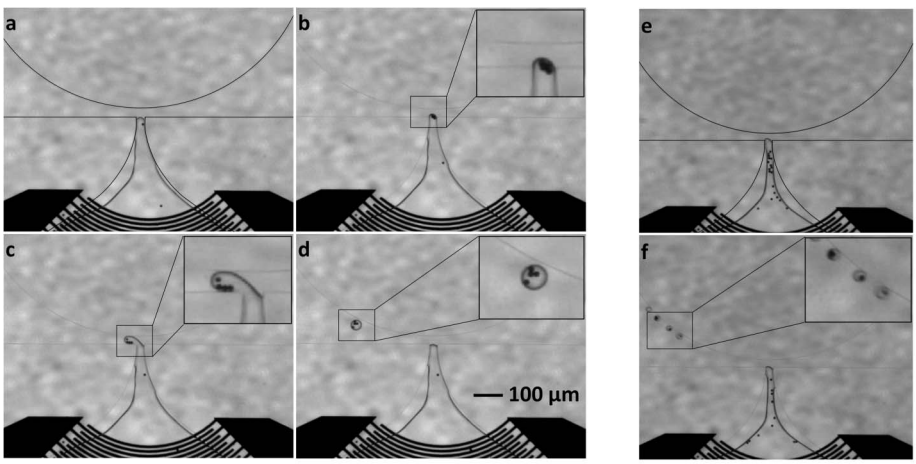

Fig. 4 Two modes of particle concentration and encapsulation during droplet production on a 95.4 MHz (40 µm wavelength) SAW device. (a–d) Discrete droplets encapsulating 10 µm particles are produced when (a) a dilute particle solution at rest is (b) excited by a low-power (1 W) SAW for a set period (2 s), concentrating particles at the interface. (c) The application of a high-power pulse (>2 W) for 100 ms is used to deform the interface, pushing it into the oil phase, which subsequently breaks off due to the pressure differential on either side of the protrusion leading to (d) a water-in-oil droplet encapsulating the particles previously concentrated at the interface. (e,f) Continuous encapsulation of individual particles occurs at higher oil flow rates and application of SAW (here 4 W). (e) The particle solution is semi-concentrated near the orifice whereupon (f) a burst of SAW creates a series of 8 pl droplets each containing one or two particles. The PDMS boundaries are highlighted in (a,e) for clarity.

Fig. 2e. Additionally, the system has the potential to generate multiple droplets with each pulse, with longer durations (>400 ms) at higher powers giving rise to additional droplets (Fig. 2f). The size of the additional droplets is determined by the specific system kinetics for a given power and pulse duration (Fig. 3). Secondary, tertiary, *etc.* droplets are generally larger, though pulse shutoff during the production of a given droplet can result in a smaller secondary droplet (Fig. 3b).

Particle concentration and encapsulation

When an acoustic wave interacts with a particle, much as when it interacts with any interface, it imparts a time-averaged force on that particle in the direction of propagation. In the case of the SAW device setup in Fig. 1 this means that particles located in water can be concentrated at the oil–water interface prior to droplet creation, resulting in an water-encapsulated particle (see Supplementary Videos 2 and 3†), a process that could easily be applied to individual cells. Fig. 4 shows two methodologies to produce encapsulated 10 μm particles. In Fig. 4(a–d) applying a relatively low-power SAW to translate particles for a short period (1–5 s) concentrates particles at the orifice, with a subsequent high-power pulse of short duration (<100 ms) sufficient to displace the interface into the oil flow sufficiently to result in droplet break-off. In Fig. 4(e,f) continuous application of SAW is used to simultaneously concentrate particles near the orifice and produce droplets. It is important to note that the frequency and particle size have significant bearing on the ability for SAW to concentrate particles at the interface. For a particle of radius R subject to a traveling acoustic wave the acoustic radiation force $F_t \sim f^4, R^6$: higher frequencies and larger particles will result in drastically more effective collection.[51] Additionally, the standing wave force for a constant pressure amplitude, where $F_s \sim f, R^3$, will overpower the travelling wave force at lower frequencies. In the setup tested here with the particle solution directly atop the interdigital transducers, a 95.4 MHz device was able to push particles to the interface, while in a 48.4 MHz device particles instead move to the standing wave nodes in between IDT finger-pairs. Most acoustic microfluidic devices utilize standing waves to manipulate particles[38,52–55] because the standing wave force is stronger for frequencies typically utilized. The application here is one of the few cases where the traveling wave force is both dominant and desired for directional particle concentration, a notable exception being a case where 140 MHz SAW was used to direct (substantially larger) ~100 μm droplets.[56] While high-frequency SAW is broadly compatible with biomolecules and cells,[34,55] thermal effects must be considered when relatively high power pulses (here up to 5 W) are used. Over an example test period used to produce droplets (5 pulses over 10 s for time-averaged power densities of 0.4 W) the temperature increase was observed to be <2 °C. For longer test periods, the thermal conductivity of the surface on which the device is placed significantly affects the steady state temperature of the device, with active thermal cooling (as in the case of a peltier cooler) limiting steady-state temperature increases by as little as <3 °C.

Conclusion

In summary, we have developed a novel system for the on-demand production of individual water-in-oil droplets using high-frequency SAW and demonstrated encapsulation of particles in vesicles. Our SAW system offers the advantage of combining droplet production, concentration and encapsulation in a single device, hence allowing direct integration with digital microfluidic devices for chemical or biological assays. Droplet creation here does not require the use of surfactants, emulsifiers or other fluid treatments that may affect chemical or cell processes, and can be powered by readily miniaturizable high-frequency power circuits. Integration of multiple devices integrated on a single platform allows simultaneous parallel processing for biochemical assays. The multiple operating modes for droplet production and particle encapsulation offered by the system presented here, including both single on-demand and continuous production, means this method can be flexibly applied to a variety of microfluidic systems.

Acknowledgements

Fabrication of the SAW actuators and device assembly was performed at the Melbourne Center for Nanofabrication.

References

1 R. Macarron, M. N. Banks, D. Bojanic, D. J. Burns, D. A. Cirovic, T. Garyantes, D. V. Green, R. P. Hertzberg, P. J. W. S. U. Janzen, P. William and G. S. Sittampalam, *Nat. Rev. Drug Discovery*, 2011, **10**, 188.
2 X. Niu, F. Gielen, J. B. Edel and A. J. deMello, *Nat. Chem.*, 2011, **3**, 437.
3 A. Wixforth, *J. Assoc. Lab. Autom.*, 2006, **11**, 399.
4 L. M. Mayr and D. Bojanic, *Curr. Opin. Pharmacol.*, 2009, **9**, 580.
5 S. S. Bithi and S. A. Vanapalli, *Biomicrofluidics*, 2010, **4**, 044110.
6 M. Sun, S. S. Bithi and S. A. Vanapalli, *Lab Chip*, 2011, **11**, 3949.
7 J. F. Edd, D. Di Carlo, K. J. Humphry, S. Köster, D. Irimia, D. A. Weitz and M. Toner, *Lab Chip*, 2008, **8**, 1262.
8 Y.-C. Tan, K. Hettiarachchi, M. Siu, Y.-R. Pan and A. P. Lee, *J. Am. Chem. Soc.*, 2006, **128**, 5656.
9 H. A. Stone, A. D. Stroock and A. Ajdari, *Annu. Rev. Fluid Mech.*, 2004, **36**, 381.
10 H. Song, D. Chen and R. Ismagilov, *Angew. Chem., Int. Ed.*, 2006, **45**, 7336.
11 M. Kiss, L. Ortoleva-Donnelly, N. Beer, J. Warner, C. Bailey, B. Colston, J. Rothberg, D. Link and J. Leamon, *Anal. Chem.*, 2008, **80**, 8975.
12 A. Doerr, *Nature*, 2005, **200**, 5.
13 M. He, J. S. Edgar, G. D. Jeffries, R. M. Lorenz, J. P. Shelby and D. T. Chiu, *Anal. Chem.*, 2005, **77**, 1539.
14 G. Christopher, N. Noharuddin, J. Taylor and S. Anna, *Phys. Rev. E*, 2008, **78**, 036317.

15 J. Xu, S. Li, J. Tan and G. Luo, *Microfluid. Nanofluid.*, 2008, **5**, 711.
16 S. Okushima, T. Nisisako, T. Torii and T. Higuchi, *Langmuir*, 2004, **20**, 9905.
17 S. Anna, N. Bontoux and H. Stone, *Appl. Phys. Lett.*, 2003, **82**, 364.
18 A. Gañán-Calvo and J. Gordillo, *Phys. Rev. Lett.*, 2001, **87**, 274501.
19 M. Pollack, A. Shenderov and R. Fair, *Lab Chip*, 2002, **2**, 96.
20 J. Ding, K. Chakrabarty and R. B. Fair, *IEEE Trans. Comput.-Aided Des. Integr. Circuits Syst.*, 2001, **20**, 1463.
21 C.-H. Chen, D. Saville and I. Aksay, *Appl. Phys. Lett.*, 2006, **89**, 124103.
22 P. Ferraro, S. Coppola, S. Grilli, M. Paturzo and V. Vespini, *Nat. Nanotechnol.*, 2010, **5**, 429.
23 M. Cecchini, S. Girardo, D. Pisignano, R. Cingolani and F. Beltram, *Appl. Phys. Lett.*, 2008, **92**, 104103.
24 A. Bransky, N. Korin, M. Khoury and S. Levenberg, *Lab Chip*, 2009, **9**, 516.
25 D. Collins, O. Manor, A. Winkler, H. Schmidt, J. Friend and L. Yeo, *Phys. Rev. E*, 2012, **86**, 056312.
26 A. R. Rezk, O. Manor, J. R. Friend and L. Y. Yeo, *Nat. Commun.*, 2012, **3**, 1167.
27 L. Schmid and T. Franke, *Lab Chip*, 2013, **13**, 1691–1694.
28 G. Hertz and H. Mende, *Z. Phys.*, 1939, **114**, 354.
29 T. Franke, S. Braunmüller, L. Schmid, A. Wixforth and D. Weitz, *Lab Chip*, 2010, **10**, 789.
30 A. Neild, S. Oberti and J. Dual, *Sens. Actuators, B*, 2007, **121**, 452.
31 S. Oberti, D. Moeller, A. Neild, J. Dual, F. Beyeler, B. Nelson and S. Gutmann, *Ultrasonics*, 2010, **50**, 247.
32 J. Reboud, Y. Bourquin, R. Wilson, G. S. Pall, M. Jiwaji, A. R. Pitt, A. Graham, A. P. Waters and J. M. Cooper, *Proc. Natl. Acad. Sci. U. S. A.*, 2012, **109**, 15162.
33 R. Walker, I. Gralinski, K. Keong Lay, T. Alan and A. Neild, *Appl. Phys. Lett.*, 2012, **101**, 163504.
34 L. Y. Yeo and J. R. Friend, *Biomicrofluidics*, 2009, **3**, 012002.
35 A. Wixforth, *Superlattices Microstruct.*, 2003, **33**, 389.
36 C. J. Strobl, Z. von Guttenberg and A. Wixforth, *IEEE Trans. Ultrason. Ferroelectr. Freq. Control*, 2004, **51**, 1432.
37 R. Shilton, M. Tan, L. Yeo and J. Friend, *J. Appl. Phys.*, 2008, **104**, 014910.
38 J. Shi, X. Mao, D. Ahmed, A. Colletti and T. Huang, *Lab Chip*, 2008, **8**, 221.
39 M. Tan, L. Yeo and J. Friend, *Europhys. Lett.*, 2009, **87**, 47003.
40 M. Tan, J. Friend and L. Yeo, *Phys. Rev. Lett.*, 2009, **103**, 24501.
41 J. Friend and L. Yeo, *Rev. Mod. Phys.*, 2011, **83**, 647.
42 J. Rooney and W. Nyborg, *Am. J. Phys.*, 1972, **40**, 1825.
43 B. Chu and R. Apfel, *J. Acoust. Soc. Am.*, 1982, **72**, 1673.
44 R. Beyer, *J. Acoust. Soc. Am.*, 1978, **63**, 4.
45 T. Hasegawa, T. Kido, T. Iizuka and C. Matsuoka, *Acoustical Science and Technology*, 2000, **21**, 145.
46 S. M. Langelier, L. Y. Yeo and J. Friend, *Lab Chip*, 2012, **12**, 2970.
47 L. Fisher, E. Mitchell and N. Parker, *J. Food Sci.*, 1985, **50**, 1201.
48 P. Garstecki, M. Fuerstman, H. Stone and G. Whitesides, *Lab Chip*, 2006, **6**, 437.
49 P. Garstecki, I. Gitlin, W. DiLuzio, G. M. Whitesides, E. Kumacheva and H. A. Stone, *Appl. Phys. Lett.*, 2004, **85**, 2649.
50 M. De Menech, P. Garstecki, F. Jousse and H. Stone, *J. Fluid Mech.*, 2008, **595**, 141.
51 L. V. King, *Proc. R. Soc. London, Ser. A*, 1934, **147**, 212.
52 A. Nilsson, F. Petersson, H. Jönsson and T. Laurell, *Lab Chip*, 2004, **4**, 131.
53 F. Petersson, A. Nilsson, C. Holm, H. Jönsson and T. Laurell, *Lab Chip*, 2005, **5**, 20.
54 X. Ding, S.-C. S. Lin, B. Kiraly, H. Yue, S. Li, I.-K. Chiang, J. Shi, S. J. Benkovic and T. J. Huang, *Proc. Natl. Acad. Sci. U. S. A.*, 2012, **109**, 11105.
55 J. Shi, D. Ahmed, X. Mao, S.-C. S. Lin, A. Lawit and T. J. Huang, *Lab Chip*, 2009, **9**, 2890.
56 T. Franke, A. R. Abate, D. A. Weitz and A. Wixforth, *Lab Chip*, 2009, **9**, 2625.